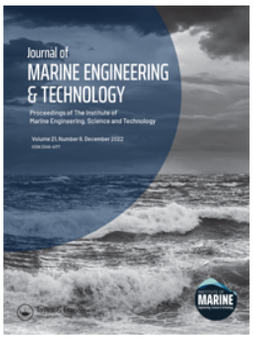

Taylor & Francis
Taylor & Francis Group

Journal of Marine Engineering & Technology

ISSN: (Print) (Online) Journal homepage: https://www.tandfonline.com/loi/tmar20

iWindCr field trial and electrochemical analysis for corrosion detection and monitoring offshore wind turbine's MP-TP steel components

S. Simandjuntak, N. Bausch, A. Farrar, Juan Ahuir-Torres I, Bob Thomas & Joseph Muna

To cite this article: S. Simandjuntak, N. Bausch, A. Farrar, Juan Ahuir-Torres I, Bob Thomas & Joseph Muna (2022) *iWindCr* field trial and electrochemical analysis for corrosion detection and monitoring offshore wind turbine's MP-TP steel components, Journal of Marine Engineering & Technology, 21:6, 311-323, DOI: 10.1080/20464177.2021.1949088

To link to this article: https://doi.org/10.1080/20464177.2021.1949088

Published online: 01 Jul 2021.

JOURNAL OF MARINE ENGINEERING & TECHNOLOGY
2022, VOL. 21, NO. 6, 311–323
https://doi.org/10.1080/20464177.2021.1949088

Taylor & Francis
Taylor & Francis Group

iWindCr field trial and electrochemical analysis for corrosion detection and monitoring offshore wind turbine's MP-TP steel components

S. Simandjuntak [a], N. Bausch [b], A. Farrar[b], Juan Ahuir-Torres I [c], Bob Thomas[d] and Joseph Muna[e]

[a]School of Mechanical and Design Engineering (SMDE), University of Portsmouth, Portsmouth, UK; [b]School of Energy and Electronic Engineering (SENE), University of Portsmouth, Portsmouth, UK; [c]Faculty of Engineering and Technology, General Engineering Research Institute, John Moores University of Liverpool, Liverpool, UK; [d]Avonwood Developments Ltd, Bournemouth, UK; [e]Avanti Communications, London, UK

ABSTRACT

A Proof-of-Concept (POC) low power-low current wireless sensor network (WSN) for corrosion detection and monitoring of offshore wind turbine (OWT)'s component, entitled *iWindCr*, has been developed and field trialled in one of the OWTs in the UK south region. This paper reports on the setting up and outcomes of this field trial. The trial has successfully demonstrated the working functionality of the WSN by measuring changes of the Open Circuit Potential (OCP) and Zero Resistance Ammeter (ZRA) electrochemical parameters over a period of time. The state of corrosion and estimated life of an M72 galvanised steel stud, part of the Monopile (MP)-transition piece (TP) flanged connection were evaluated using the real-time data from the WSN with reference to the material's corrosion thresholds from the *iWindCr* database. The paper details the electrochemical analysis processes in relation to the Electrochemical Impedance Spectroscopy (EIS), Potentiodynamic Polarisation Curve (PPC) in addition to the OCP and ZRA techniques. The electrochemical parameters and corrosion threshold values from seawater immersion tests of the steel alloys SS316L and S355, the typical MP-TP materials are presented.

ARTICLE HISTORY
Received 4 March 2021
Accepted 24 June 2021

Nomenclature

E	potential
E^o	standard potential
R	gas constant (8.314 J mol^{-1} K^{-1})
T	temperature
n	number of electrons transferred in the corrosion reaction
F	Faraday constant (96485 C/mol)
C_o	the oxidised species concentration
C_r	the reduced species concentration
n_o and n_r	stoichiometric factor of the oxidised species and of the reduced species, respectively
I_{corr}	corrosion current density
I_o	current density amplitude
R_p	polarization resistance
β_c	cathodic Tafel slope
βa	anodic Tafel slope
$Z_{(f)}$	impedance at a frequency
F	frequency
t	time
θ	shift phase
$R_{(f)}$	resistance at a frequency
$C_{(f)}$	capacitance at a frequency
F_{max}	frequency at maximum shift phase
I_n	stable current density at a certain number, n of measurement
R_n	noise resistance
σ_E	potential standard deviation
σ_I	current density standard deviation
$L.I.$	localised index
$I_{R.M.S.}$	root mean square of the current density
CR	corrosion rate
M	molecular mass
A	exposure area
P	density of the (oxidised) material
I_c	cathodic current density
I_a	anodic current density
$E_{applied}$	applied potential
ΔE_p	passive potential range
E_{bp}	breakage passive film potential
H	type of element
Z	number of time constant
$Zmod$	impedance modulus

List of Abbreviations

POC	proof-of-concept
WSN	wireless sensor network
OWT	offshore wind turbine
OCP	open circuit potential
ZRA	zero resistance ammeter
MP	mono-pile
TP	transition piece
EIS	electrochemical impedance spectroscopy
PPC	potentiodynamic polarisation curve
SS316L	stainless steel 316L
S355	Steel 355
UK	United Kingdom

CONTACT S. Simandjuntak Sarinova.simandjuntak@port.ac.uk School of Mechanical and Design Engineering (SMDE), University of Portsmouth, Anglesea Road, Portsmouth PO1 3DJ, UK

O&M	operation and maintenance
GBS	gravity-based structure
RTRS	real-time remote sensing
IoT	Internet of Things
M72 10.9	Galvanised Steel
EN	electrochemical noise
PEEK	poly ether ether ketone
PCB	printed circuit board
S235	Steel 235
SS	salt spray
GL	grease lubricant
OL	oil lubricant
Ag/AgCl	silver/silver chloride potassium chloride saturated
Sat. KCl	
RMS	root mean square
SD	secure digital

1. Introduction

An increasing number of offshore wind turbine (OWT) installations in various countries and locations has showcased the attention and commitments of many countries worldwide including the United Kingdom (UK) on the provision of clean, renewable and affordable, yet secure energy generation (GWEC 2017). In Europe, the investments in new OWTs amounted to €10.3bn, a 37% increase from 2017 (Wind Europe 2019). As published in the UK Wind Energy Database, the advantage of UK's geographical location has led to 2016 wind turbines of 37 offshore operational (> 100 kW) projects, and the number continues to rise (UKWED 2019). RenewableUK (2019) reported that these OWTs already powered the equivalent of 4.5 million homes annually and the UK recently announced plans to quadruple offshore wind power by 2030. The OWT's development characteristics such as wider space and span for installation reduced visual and environmental impacts, and zones with elevated wind rate indeed favour the faster growth rate. However, they also have contributed to more challenges with respect to their design, installation, operation and maintenance (Estate 2010) (Burton et al. 2011) (Umaya et al. 2013) (DNV 2013). The remote locations, tall structures and the harsh conditions from the marine environment such as saltwater and moisture (salt spray/fog), erosive elements (from wind and wave), ultraviolet light (direct sunlight) and biochemical products from marine growth contribute to some of the challenges in the OWT's operation and maintenance (O&M). The effective and correct O&M approaches to face the challenges are therefore crucial for maintaining the reliability and the structural integrity of the OWTs.

The OWT's key structures are the foundation, turbine tower, nacelle and rotor blades, where the foundation and turbine tower make up the main support parts. The foundation, that is, essentially located below and at the water level, will direct the loads onto the support structure into the seabed. A Monopile (MP), manufactured from rolled steel plates and welded together to form a cylindrical section, is the most frequently used type among others such as tripod, jacket and Gravity-Based Structure (GBS), and floating foundation (Estate 2010) (DNV 2013) (Arshad and O'Kelly 2013). The foundation and the tower are connected by a transition piece (TP) where a work/service platform (and access to the tower) would be located (Figure 1). Most MP's parts/structures are subjected to full immersion in seawater (known as submerged zone) and some parts of MP-TP connection are exposed to wave (known as splash zone). Nearer to the service platform in the internal part of the MP-TP, where parts/components are positioned to be slightly above the splash zone, they are likely to be exposed to moisture and/or salt spray.

Structural steels such as S355 are one of the most typical materials selected for the MP due to its resistance to corrosion in seawater. Other materials such as stainless steel SS316L and 10.9 Galvanised steel alloys are also commonly used in parts/components of the MP, TP, and tower. Those parts/components made of these materials are often given an additional corrosion protection such as using coating and sacrificial anodes (DNV 2016). Although the majority of the OWT installations have less than 10 years in operation, some of the

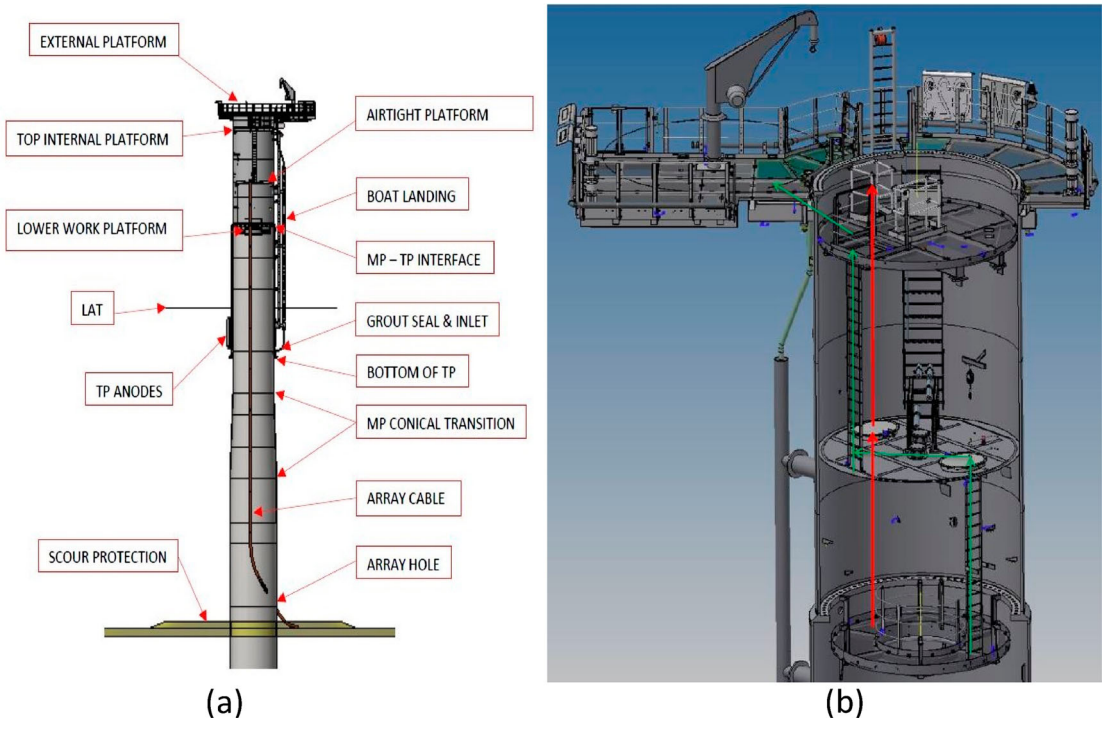

Figure 1. Schematic of the (a) external and (b) internal MP-TP of a wind turbine (*courtesy of Rampion Wind Farm*).

parts/components made of these materials were reported to already experience corrosion (Perälä 2010; Black et al. 2015; Pawsey 2016; Weinell et al. 2017; Price and Figueira 2017).

With the support structure's cost of around 25% of the total offshore WT's, there is a real need and urgency in preventing and monitoring the threats to the integrity of the OWTs such as corrosion. This can be done through the implementation of a cost-effective Real-Time Remote Sensing (RTRS) system. Due to the accessibility issues to some parts/components of the OWTs and to the power supply, such a system would need to be small, flexible and comprised of self-sustained low powered sensor and sensor interface as well as a wireless communication link.

These design considerations have been applied to the *iWindCr system*, and were one of the objectives of this technology development project funded by the Innovate UK. The system was developed to comprise a wireless sensor network (WSN) system consisting of smart miniaturised sensors that employed the electrochemical techniques in this case the Open Circuit Potential (OCP) and the Zero Resistance Ammeter (ZRA) for corrosion detection and monitoring. Further details on the design approach are available in (Ahuir-Torres et.al. 2019a, J. of Wind Energy). The concept of Internet of Things (IoT) was also adopted to incorporate the WSN with satellite and terrestrial communication networks, giving an assured capability and agreed protocol for data backhaul from the remote offshore wind turbines to the control room. The cyclical transmitted data would be monitored and used as indicators or references to pinpoint the event and type of corrosion when it occurs. As an alternative, without satellite bandwidth connectivity, the data could be stored locally on a storage medium such as using an SD card, which can then be retrieved periodically for analysis or accessed remotely via the user interface if connected to the internet using a terrestrial connection. The latter option was adapted for the *iWindCr* field trial.

At the moment, *iWindCr* project did not look deeply into the underwater WSN communication (beyond its scopes). The authors are however aware that recently, Gupta and Goyal (2021) and Goyal et al. (2021) have investigated methods for communications in underwater wireless sensor networks such as the Hop-by-Hop Vector-Based Forwarding (HH-VBF), one of the models for data gathering and Depth-Based Routing (DBR) for data routing optimisation. These methods could address the challenges around underwater WSN communications that are mainly due to the unpredictable nature of the environment such as temperature and water current (flow speed) fluctuations. Thus, they would be considered in the future development of the *iWindCr* system

iWindCr was trialled in one of the 116 OWTs in a windfarm in the UK's south region. This field trial was used to test the system's working principal and the reliability of the data acquisition by verifying the adequacy of data readings in connection to the *iWindCr* sensor interface setting that is, the frequency of sensor readings and the data quality needed for the OCP and ZRA analysis. Subsequently, the system was used to monitor electrochemical changes to assess corrosion activities in one of the 84 studs, manufactured from10.9 Galvanised Steel (M72), in the MP-TP flanged connection of the OWT.

iWindCr also had in its programme the in-house testing to determine the corrosion parameters and their threshold values according to the specification or test conditions and environment as close as to those reported in the literature and in the relevant international testing standards (Ahuir-Torres et al. 2019b, DIB). The relationship of the data readings from the *iWindCr* system to materials' thresholds values would allow for the identification of a certain type and characteristic of corrosion. As a further output, the *iWindCr* project has thus led to the creation of a database of various materials' corrosion parameters and thresholds that can be utilised by end-users

Figure 2. *iWindCr* system set-up in the MP-TP flanged connection location with the sensor attached to the M72 stud on the right.

Table 1. PEEK sensor characteristic.

Size: Length × Width × Thickness (in cm)	1.0 × 1.0 × 0.15
Exposed Area (cm^2)	1
Molecular Mass (g/Mol)	55.8
Density (g/cm^3)	8.05
Oxidation State (e-)	3

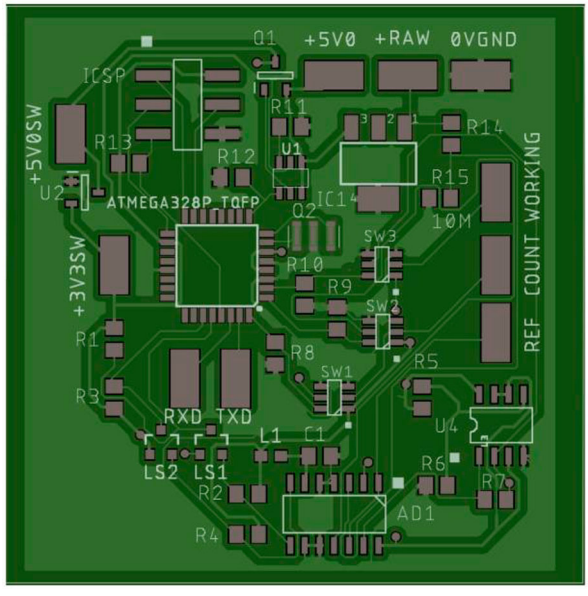

Figure 3. The sensor interface PCB layout.

such as wind farm owners or managers and inspectors to assess corrosion occurrence. After conducting onerous laboratory testing and a comprehensive electrochemical analysis, it was concluded that a generic solution for corrosion detection in the tower and foundation components or structures would be impractical or unviable to be established. Hence, their corrosion occurrences will be strongly dependent on its materials and the environment that these materials are exposed environment.

The data generation process employs well known electrochemical analysis techniques such as Electrode Impedance Spectroscopy (EIS),

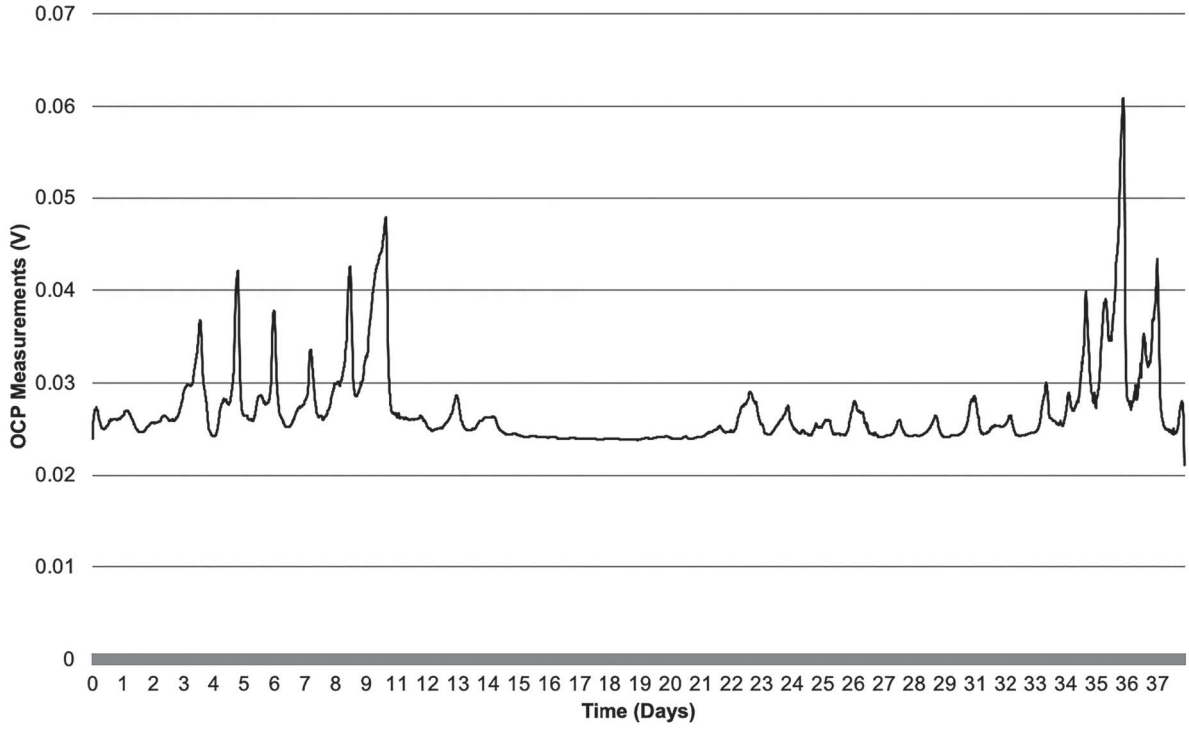

Figure 4. OCP Voltage Real Time Reading.

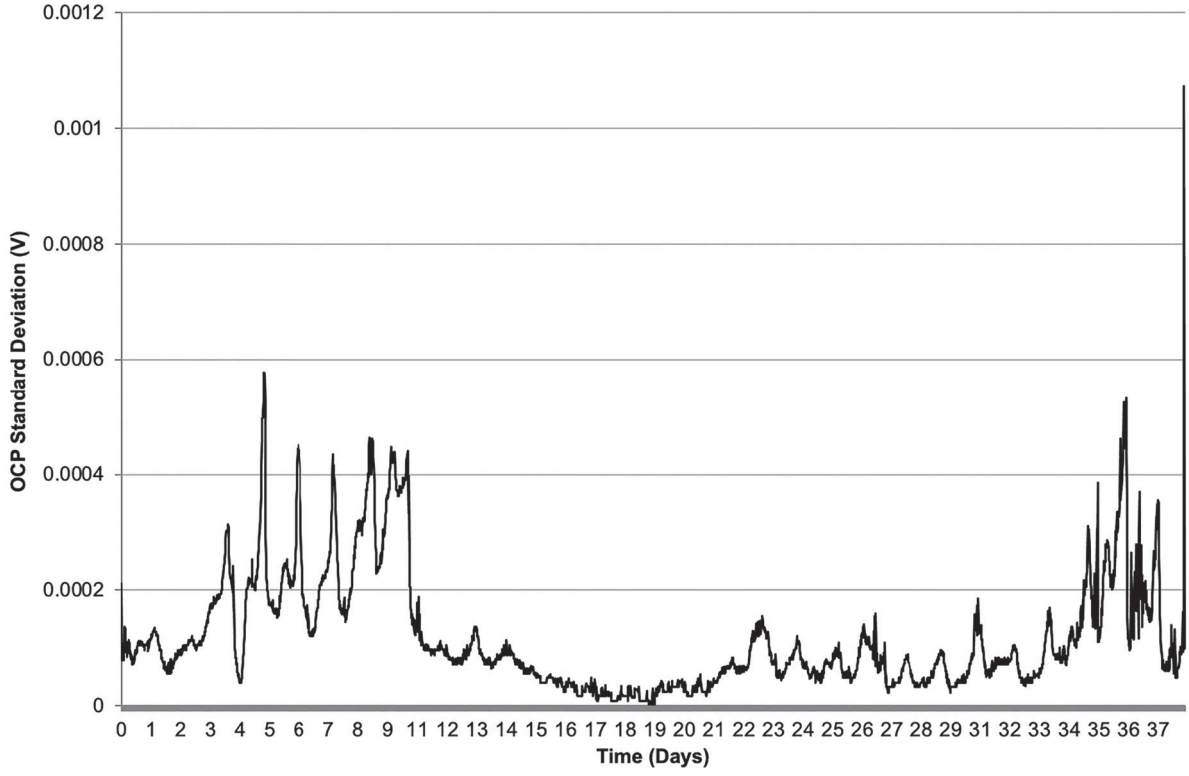

Figure 5. OCP Voltage Standard Deviation Real Time Reading.

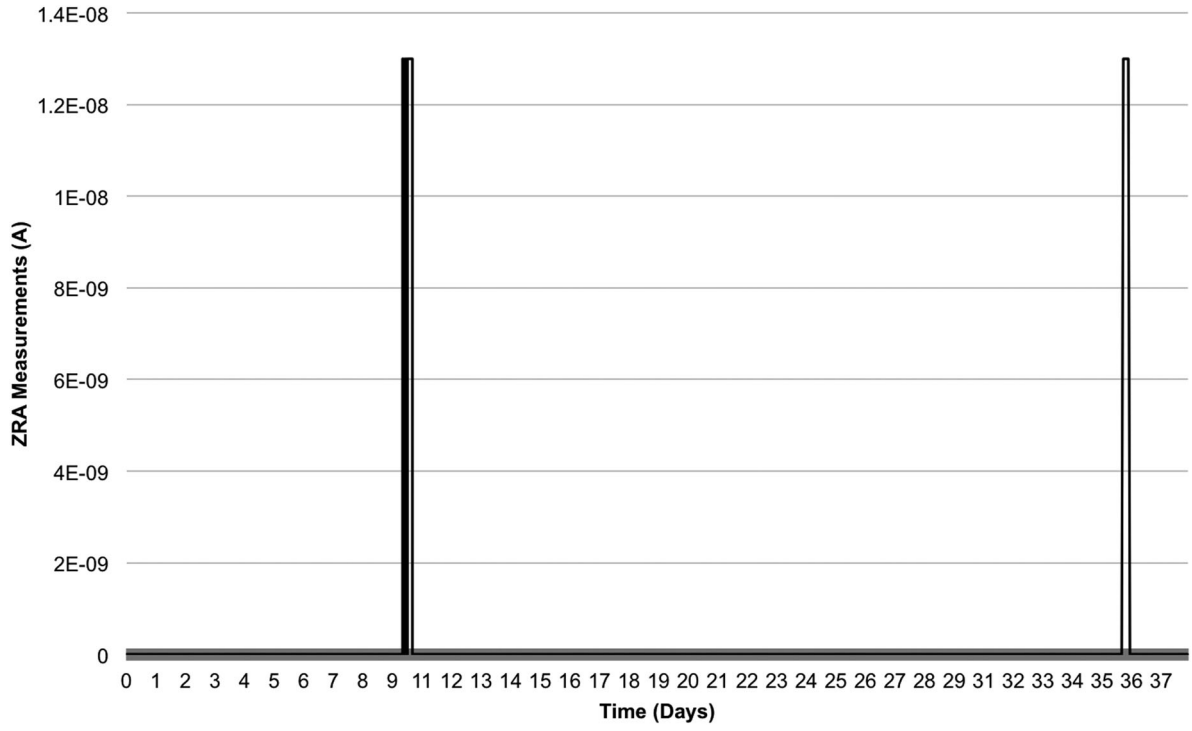

Figure 6. ZRA Current Reading.

Potentiodynamic Polarisation Curves (PPC), Electrochemical Noise (EN), in addition to OCP and ZRA. The details of these techniques can be found in (Shreir 1994), (McCafferty 2010), (Murata 2017) and many more handbooks/literatures.

This paper consists of two discussion parts. The first part discusses the setting and outcomes of the field trial. The second part details the corrosion thresholds' determination process of steel alloys SS316L and S355 using these techniques and presents their results.

I. iWindCr's Field Trial

Set-up: Sensor and Sensor Interface

The sensor system was mainly comprised of a polymer-based sensor made of Poly Ether Ether Ketone (PEEK), a 50 mm (length) × 50 mm (width) × 2.0 mm (thickness) Printed Circuit Board (PCB), an SD card, and a battery to power up the system for an approximately four weeks duration. Figure 2 shows the *iWindCr* sensor attachment on one of the M72 studs. It was attached directly onto the M72 stud (on a clean unpolished surface) using silver conductive epoxy adhesive. Although a chemical compositional analysis would be needed to confirm it, the OWT operator informed that the studs could have been coated with Molykote® coating (www.dupont.com).

The characteristics of the sensor are tabulated in Table 1. The sensor was manufactured to include a three-electrode cell system which are one working, one counter and one reference electrodes, using silver and copper wires. It was attached directly onto the M72 stud (on a clean unpolished surface) using silver conductive epoxy adhesive. The polymer sensor was connected to the PCB using the three-electrode cell system's wires. Figure 3 represents the PCB layout which would host the power supply connection pads, switch and regulator; XBee wireless communication modules; analogue to digital converters; the OCP and ZRA modules and mode switches; programming port; microcontroller for sensor readings and nanotimer. A description on the design of the sensor and PCB layout can be found in (Ahuir-Torres et.al. 2019a, J. of Wind Energy). For this trial, a nano-timer was used to manage data collection, set up to run for 200 s at every 15 min interval. The selected times were based on laboratory performance tests of the sensor system, where a minimum of 50 datapoints per reading within a period of no less than 120 s was needed to obtain a valid and reliable OCP and ZRA results for the electrochemical analysis. During this test, a current of 100 nA was measured (using Keithley Pico-ammeter Model 485) whilst the system was idle, and a maximum current of approximately 8 mA when the micro-controller was switched on briefly for approximately 100 ms before it settled to a 5 mA current during reading at the given interval of no less than 120 s. Figures 4–6 show the voltage (V) and current density (A/cm^2) reading profiles (using raw data) from the ~ 30 days trial. Figure 4 demonstrates the evolution of the potential with time. The potential fluctuated with the time between 0.025 and 0.060 V in the beginning (from 0 to 13 days) and at the end (from 22 days to 37days) in the duration of the experiments. Whilst during the middle stage (from 14 days to 22 days), the potential remained constant at 0.025 V. The graph in Figure 5 shows the potential standard deviation with time which is used to check the accuracy or stability of the sensor reading. The low values of the potential standard deviation (from 0 V to 0.0006 V) were recorded. The fluctuation of these values would indicate unstable chemical reactions. The current overtime reading is presented in Figure 6. The current and therefore the current density remained to be zero with time to the exception of the ninth and tenth day, when it was increased to 14 nA/cm^2. These increments of the current could be caused by a low-level oxidation reaction.

Data analysis

Table 2 summarises the *iWindCr* system's trial setting and outcomes. The average voltages and current densities from the field trial were compared with the threshold values of the 10.9 Galvanised Steel (M72) obtained from the laboratory seawater immersion corrosion tests. It was understood however that due to the position of the studs on the MP-TP connection area (above the splash zone), they

Table 2. Summary of the *iWindCr* system's trial setting and outcomes.

Setting & Outcomes	Value
Nanotimer wake up interval (average, second)	886
Sensor interface uptime (minimum, second)	250
Total time between reading (second)	1136
Average Potential (V)	2.697E–02
Standard Deviation Potential (V)	3.704E–03
Average Current Density (A/cm^2)	1.720E–10
Standard Deviation Current Density (A/cm^2)	1.485E–09

Table 3. Steel Alloy's Corrosion Threshold Values and Trial's data reading comparison.

Alloy	Environment	Potential (V)	Current density (A/cm^2)
M72 stud	Salt Spray (SS)	0.0270	1.7E–10
10.9 Galvanised Steel	Sea Water Immersion (SW)	≤ -1.000,	$\geq$ 8E–05
SS316L	SS	$\leq$ 0.030, $\geq$ 0.050	$\geq$ 2E–09
S235	SS	≤ -0.390 ≥ -0.120	$\geq$ 2E–07
	Grease Lubricant (GL) at 298 K	≤ -0.120, $\geq$ 3.000	$\geq$ 2E–09
	Oil Lubricant (OL) at 298 K	$\leq$ 1.180, $\geq$ 3.000	$\geq$ 2E–10

would never be fully immersed. Instead, they would be exposed to salt spray and moisture. The trial results on M72 stud were understandably not in agreement with the corrosion threshold values of the M72 data determined from the fully immersed corrosion (laboratory) tests. The potential and current density values recorded from the trial are between 0.02 and 0.06 V and between 14 nA/cm^2 and 0A/cm^2, respectively. A corrosion process could have taken place under the condition of immersion in seawater in this case, if the potential value was ≤ -1 V and the current density ought to be $\geq 80\ \mu$A/cm^2 (according to Table 3 seawater immersion M72 data).

The trial's low current density and potential values are typical values of those corrosion thresholds obtained when thin protective or passive films were present either from coating or from an artificial barrier such as from grease/lubricants on the surface of a material. Due to the possibility of a protective (Molykote®) coating being present on the stud's surface, the average voltage and current density values from the trial appeared to be more in line with those of the alloys that have protective or passive films. The results were therefore compared against the S235 data generated from tests in Grease Lubricant (GL) media/environment and Oil lubricant (OL). The environment of the GL and OL was considered to provide the protective environment as that of the Molykote®. Table 3 shows that the trial values have followed a similar trend/profile of the potential and current density of the non-corroded S235 derived from the testing in the GL environment (with the potential values ranges from -0.120 V to 3.000 V and current density of ≤ 2 nA/cm^2 for a non-corroded sample at 298 K).

For a comparison, Table 3 also shows the salt spray (SS) test results of SS316L and S235. The S316L non-corroded sample's potential value and current density would be between 0.03 and 0.05 V and ≤ 2 nA/cm^2 respectively. Although the trial's voltage reading was in the range of the SS316L potential threshold values, the current density from the trial was relatively higher than that of the SS316L value. Meanwhile, the S235 non-corroded sample's current density (≤ 200 nA/cm^2) is relatively in agreement with the trial's current density result, its voltage threshold range (between -0.39 V and -0.120 V) was nowhere close to the trial's voltage values.

Table 4. Chemical composition of the investigated metallic materials (% by mass).

Material	Fe	Al	C	Mn	Si	*P*	S	Cr	Mo	Ni	N	Cu	Mg	Zn	B	Other
SS316L	Bal.	–	0.030	2.000	0.750	0.045	0.030	16.000 – 18.000	2.00 – 3.00	10.00 – 14.00	0.010	–	–	–	–	–
S355	Bal.	–	0.220	1.600	0.550	0.030	0.03	–	–	–	–	0.550	–	–	–	–
10.9 Galvanised Steel	Bal.	–	0.200–0.550			0.025-0.040	0.025–0.050		–	–	–	–			0.003	

Table 5. Chemical composition of the artificial seawater according to *ASTM D1141-13* (g/L) (ASTM 2013).

NaCl	$MgCl_2$	Na_2SO_4	$CaCl_2$	KCl	$NaHCO_3$	KBr	H_3BO_3	$SrCl_2$	NaF	$Ba(NO_3)_2$	$Mn(NO_3)_2$	$Cu(NO_3)_2$	$Zn(NO_3)_2$	$Pb(NO_3)_2$	$AgNO_3$
24.530	5.200	4.090	1.160	0.695	0.201	0.101	0.027	0.025	0.003	9.940E-5	3.400E-5	$3.080*10^{-5}$	$9.600*10^{-6}$	$6.600*10^{-6}$	$4.900*10^{-7}$

Table 6. Electrochemical analysis techniques, corrosion output parameters and solutions.

Techniques	Analysis	Equations/Solutions
OCP	Provide information of a fresh metal corrosion potential; not suitable for determining the rate of corrosion	$E = E^o + \frac{R\times T}{n\times F}\log\left(\frac{[C_O^{no}]}{[C_r^{nr}]}\right)$
ZRA	Measure directly the stable current density in a corrosion system	$I_{corr} = I_{R.M.S} = \sqrt{\frac{\sum_1^n I_n^2}{n}}$
EIS	Allows the study of capacitive, inductive, and diffusion processes taking place in the electrochemical cell and therefore can be used to determine when breakage of the passive film or a localised corrosion has occurred	$Z_{(f)} = \frac{E_o\times\sin(2\times\pi\times f\times t)}{I_o\times\sin(2\times\pi\times f\times t+\theta)}$ $\underset{\theta=0}{\Rightarrow} R_{(f)} = Z_{(f)} = \frac{E_o}{I_o}$ $\underset{\theta=max}{\Rightarrow} \frac{1}{C_{(f)}} = 2\times\pi\times f_{max} * R_{(f)} = Z_{(f)} = \frac{E_o}{I_o\times\sin(\theta)}$
PPC	Determine the safety or passive potential range, ΔE_p. ΔE_p is the electrode potential range between the E_{corr} and the breakage passive film potential, E_{bp}. The E_{bp} is the applied electrode potential in the anodic part that causes a sudden increase of the anodic current density, I_a.	$E_{applied} - E_{corr} = \beta_c \log\left(\frac{I_c}{I_{corr}}\right) + \beta_a \log\left(\frac{I_a}{I_{corr}}\right)$
EN	Differentiate between the general/uniform and localised corrosion and can identify the distinct kind of localised corrosion, such as inter-granular, pitting or galvanic	$R_n = \frac{\sigma_E}{\sigma_I} L.I = \frac{\sigma_I}{I_{R.M.SI}}$

This trial, therefore, shows that at least two of the corrosion threshold parameters should be referred to and compared with for a more reliable corrosion detection. This emphasises the importance of corrosion threshold data generation. The salt-spray testing on the M72 will thus be carried out to validate the test further, which will be included in the *iWindCr* system future development programme.

The field test average current density and sensor characteristic values are given in Table 2 could also be used to estimate the corrosion rate, *CR* (cm/s). The *CR* is derived using Equation (1).

$$\mathrm{CR} = \frac{I_{Ave} \times M}{F \times n_e \times \rho} \tag{1}$$

where M is the molecular mass (g/mol), F is the Faraday constant (96,485 C/mol), n_e is the number of transferred electrons in redox reaction and ρ is the material density (g/cm^2).

The calculation using the trial's data estimated a very low corrosion rate (4.1401E–15 cm/s), indicating that there was no accelerated corrosion monitored during the trial. Although it has been shown in this paper that *iWindCr* system could be used to estimate the corrosion rate hence predict the life of a component, this work was performed for the purpose of *iWindCr* system functionality's demonstration only and should not be used for the structural judgment of WTs.

Corrosion Thresholds Data Generation

Experimental Setup

The chemical compositions of the investigated metallic materials, in this case: SS316L, S355 and 10.9 galvanised steel are listed in Table 4. For the laboratory corrosion testing and electrochemical analysis, test samples of 2 cm × 2 cm × 0.3 cm were manufactured from the as-received materials and manually ground using SiC paper and polished to obtain a scratch free surface and to a mirror finish. For the polishing used a dissolution mixture of colloidal silica gel (0.06 µm colloidal silica gel) 10%: 90% (V/V) distilled water was used. These non-corroded samples were cleaned after each step via commercial detergent, distilled water, iso-propanol and subsequent drying with hot air.

The corrosion testing of samples was conducted at room temperature in artificial seawater, supplied by *ReAgent Chemical Limited*, prepared in accordance with the ASTM D1141-13 (ASTM 2013). Table 5

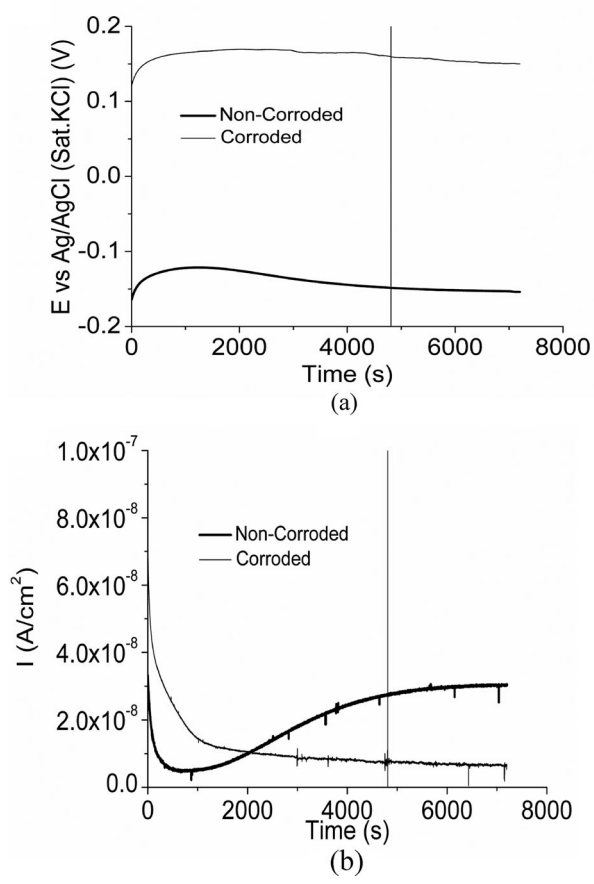

Figure 7. Electrochemical Analysis of the SS316L from seawater immersion testing using (a) OCP, (b) ZRA, (c) EIS and (d) PPC techniques

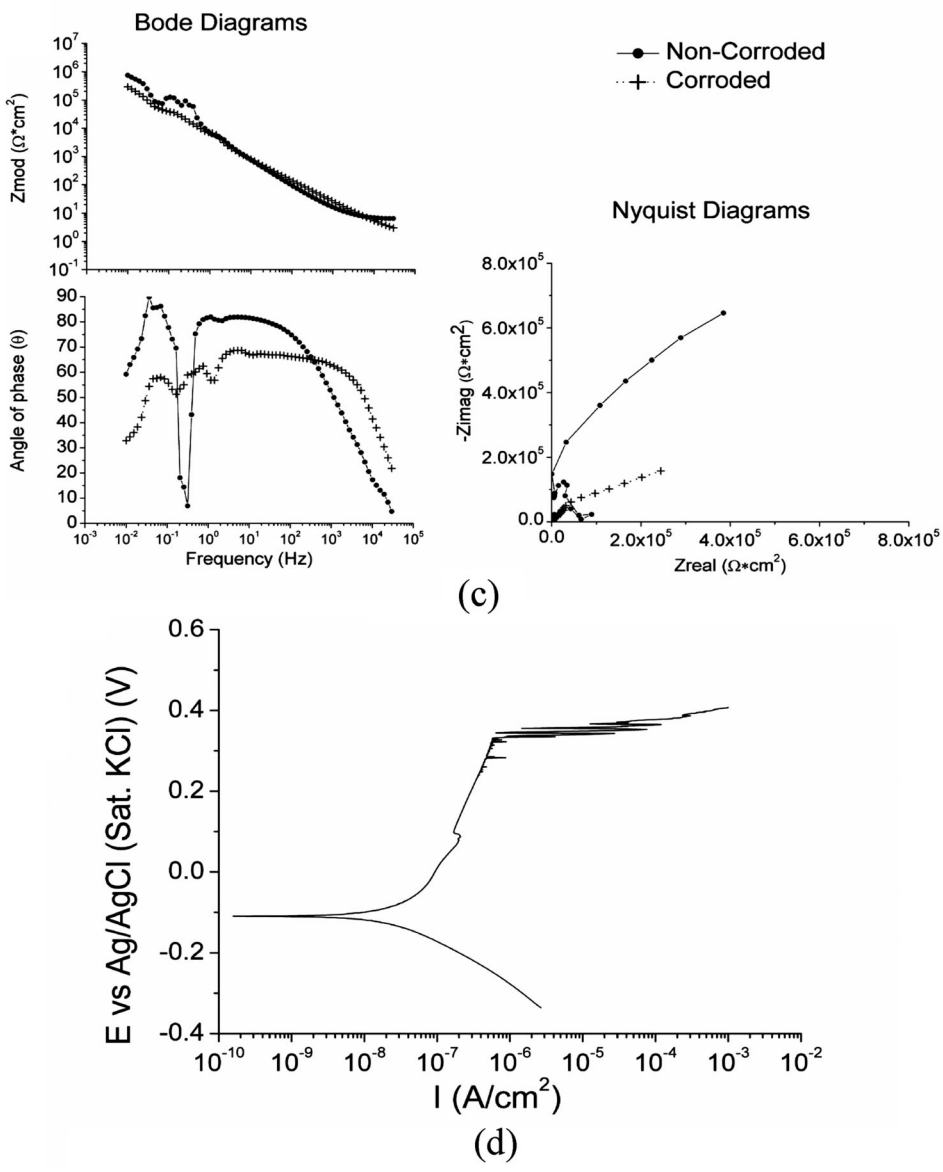

Figure 7. Continued

shows the composition of the artificial seawater. For the electrochemical process, a GillAC (ACM Instruments Software: Gill AC serial no 600) was used to control the Potentio/Galvanostat and a three-electrodes set up was employed. The test sample's area exposed for the electrochemical analysis was $\sim 0.5\ cm^2$. The corrosion processes of the samples were analysed by means of the following electrochemical analysis techniques: OCP, ZRA, EIS, EN, and PPC, summarised in Table 6 alongside their relevant parameters and solutions. The OCP and ZRA utilise two working electrodes and one reference electrode whilst the EIS and PPC employ one reference, one counter and one working electrodes. Silver/silver chloride potassium chloride saturated (Ag/AgCl Sat. KCl) was the reference electrode chosen for all the conducted electrochemical analysis techniques. The test sample was used as a working electrode and rod graphite was chosen for the second Working as well as the counter electrode.

The process sequence of the electrochemical analysis was as follows.

(i) OCP and ZRA were carried out at the same time and under the same conditions, that is, 10 Hz frequency (0.1s data acquisition) in 2 h.
(ii) EIS, PPC and EN analysis were to follow prior to the evaluation of the corrosion output or threshold values of the metallic materials.
   (a) EIS applied a 0.01–30,000 Hz frequency range, 10 points/decade to obtain 70 total points, and a potential amplitude of 10 mV Root Mean Square (R.M.S).
   (b) PPC was conducted to accelerate the corrosion (used to produce *corroded samples*) using a sweep rate of 0.167 mV/s, 10 mA/cm^2 current density limit, at an open circuit potential of −0.3 V initial potential and a final potential of 3 V against the reference electrode potential.
   (c) The analysis of the EN would be followed by utilising the ZRA and OCP data to derive the RMS current density ($I_{R.M.S}$), noise resistance (R_n) and Localised Index ($L.I$).

The above process was followed in the analysis of the non-corroded (as-received) samples and the corroded samples (after subjected to the accelerated corrosion using PPC). All testing was carried out three times or more to verify the veracity of the results obtained via the electrochemical analysis techniques. In addition, some were validated against data from tests generated using industrial or academically accepted standards found in published literature or report. Further details and references to these data can be found in (Ahuir-Torres et.al. 2019, J. of Wind Energy and DIB).

Electrochemical analysis

From the electrochemical analysis of SS316L and S355 following a fully immersed in artificial seawater corrosion testing, the outputs derived from (a) OCP, (b) ZRA, (c) EIS and (d) PPC techniques are represented in Figures 7 and 8.

Figures 7(a) and 8(a) represent the changes in the potential over time derived from the OCP analysis for both non-corroded and corroded SS316L and S355 samples, respectively.

For the case of SS316L alloy, the non-corroded and corroded samples exhibited similar evolution stages and behaviours though at different values indicating electrochemical changes on the surface of a component detected by the sensor. The first stage of corrosion process often starts with the formation of the protective oxidised (passive) film on the non-corroded sample surface, and re-passivation or reformation of passive film on the corroded sample surface. Thus, there was a rapid increase in potential observed during the first 200s in both samples. This was followed by a period when the potential showed little change or remained constant. This occurred due to the saturation or stable growth of the film, therefore no changes in its thickness and chemical composition. Following that, a slow decrease in the potential downwards was observed. The decreasing potential could occur due to several reasons. One of the reasons was due to the reduction of the resistance as a result of damage of the passive film (Compere and Le Bozec 1997) (Xin and Li 2014)

For the S355 case, a rapid decay of the potential was observed for both non-corroded and corroded samples. This could be a result from the high reactivity of S355 with the environmental oxygen. The S355 is unviable to produce a passive film and therefore, the oxygen is free to directly react with the metal (Shreir et al. 2010) (Gassama et al. 2015). Non-corroded sample potential continued to reduce but at a lower rate. Potential decay was until −0.547 V after 5200s of immersion. The reduction of the slope was thought to occur due to the losses of metal reactivity over time. S355 corrosion generated products that were deposited on surfaces and impeded the oxygen access to the bare metal, hence reduced the corrosion reaction (Shreir et al. 2010) (Choudhary et al. 2016).

In the case of corroded samples, the potential slowly increased with the immersion time until hitting a value of −0.577 V at 1900s. This occurred due to the increase in the corrosion resistance of the metallic alloy. The slight increase in the resistance was associated with the deposition of the unstable corrosion products (rust). The potential remained constant (at −0.570 V) until the end of testing because the corrosion reaction has likely reached an equilibrium.

Figures 7(b) and 8(b) represent the current density evolution with time from the ZRA analysis for both non-corroded and corroded SS316L and S355 samples, respectively.

In both non-corroded and corroded samples of the SS316L, the current density decreased over time in the first second of immersion. This was associated with the fast growth of a passive film or re-passivation of the film of which increased the sample's corrosion resistance (Al-Fozan and Malik 2008;Sun 2010). The current density continuously decreased for both samples at a lower rate as the passive films on both samples began to stabilise. The current density for the non-corroded sample remained constant at 5.730×10^{-9} A/cm^2 from 560s to 1200s which could be encouraged by a constant reaction of the passive film with the aggressive environment (Estupiñán-López et al. 2011). This was followed by a slight increase in the current density to reach a value of 2.730×10^{-8} A/cm^2 after 5000s of immersion. Trans-passivation process was possibly the reason of this increase although passive film damages could also be another reason (Wharton and Wood 2005). Meanwhile, the current density of the corroded sample continued to decrease but at a very low rate before reaching a steady current density of 7.000×10^{-9} A/cm^2.

The evolution of the current density over time was different for the S355 samples. Current density measured from the non-corroded sample declined over time up to the 470s of immersion and continued to fall but at a reduced rate. The deposition of corrosion products in the formation of a passive film was thought to lower the rate of decline. Corroded samples also exhibited a rapid decay of the current density in the first seconds of testing but were only up the 120s of immersion time. The current density then increased over time reaching 1.300×10^{-3} A/cm^2 at the end of the test. This could be caused by the formation of damaged or non-adherent corrosion product or passive film (Shreir et al. 2010) (Murata 2011).

Figures 7(c) and 8(c) show the representations of the Bode and Nyquist diagrams of the SS316L and S355 alloys, respectively.

These diagrams were used to determine the electrochemical parameters. These parameters include the dissolution resistance (R_s), the resistance at the interface that was formed between porous and aggressive species (R_{po}) and its associated capacitance (C_{po}), the charge transference resistance (R_{ct}) and the capacitance resistance

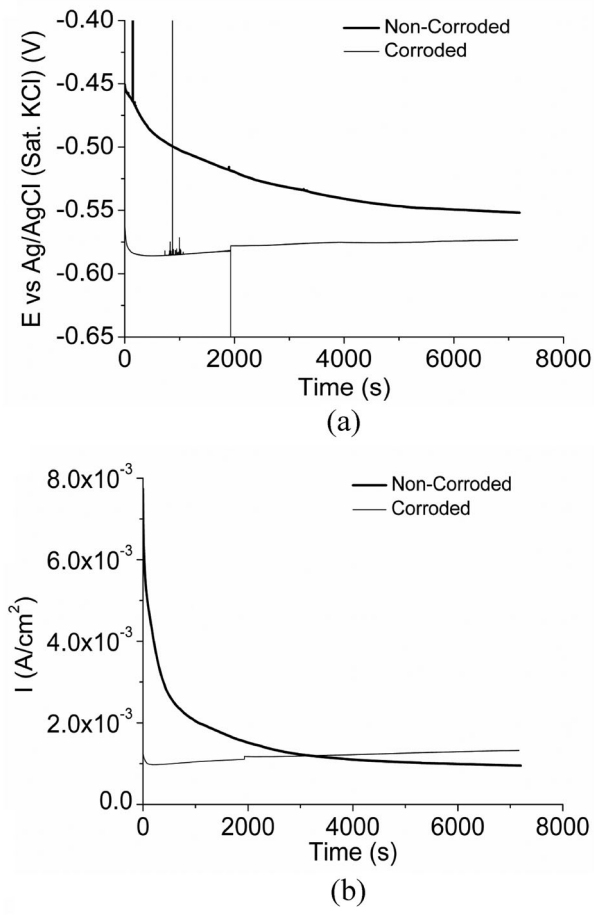

Figure 8. Electrochemical Analysis of the S355 from seawater immersion testing using (a) OCP, (b) ZRA, (c) EIS and (d) PPC techniques

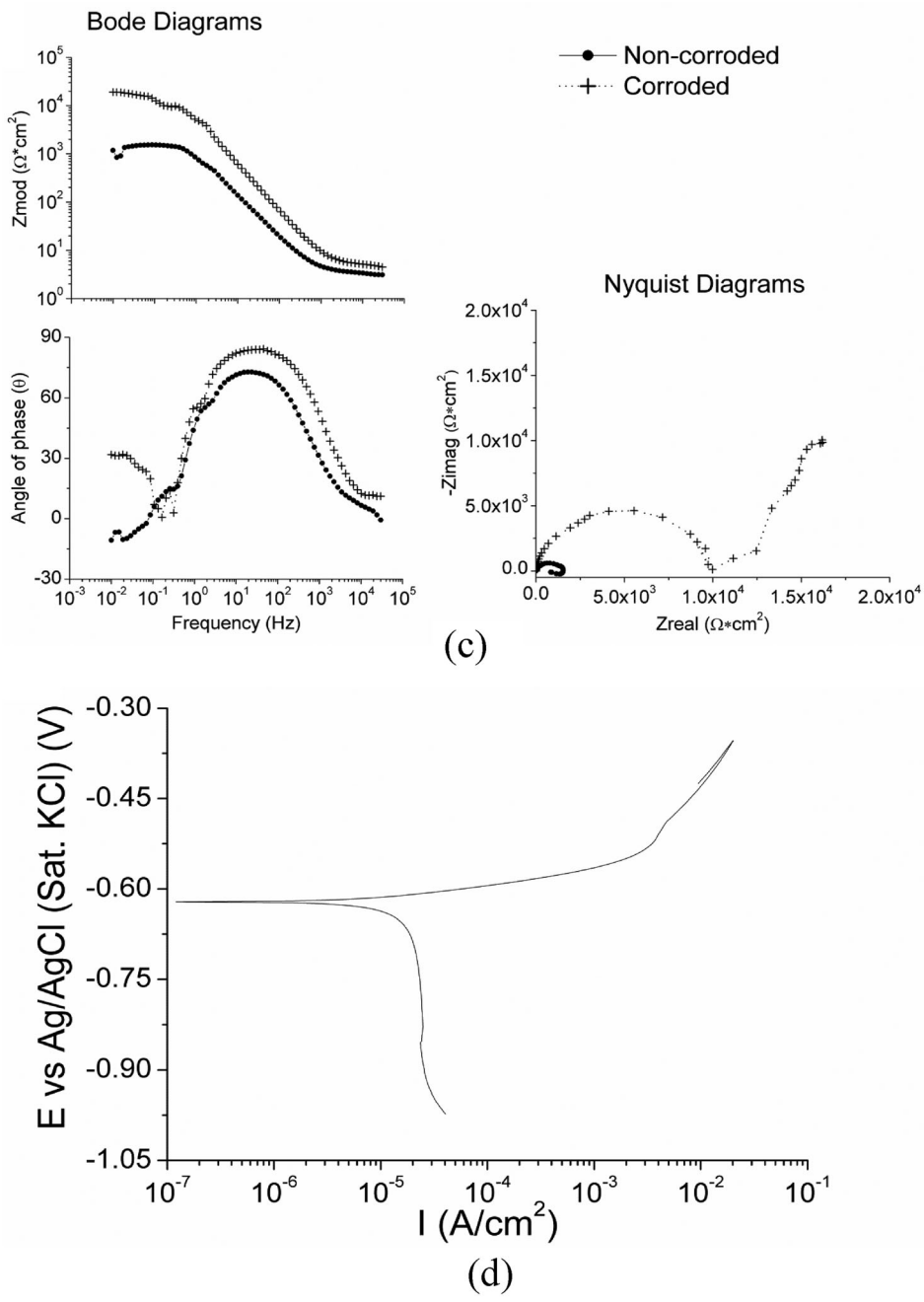

Figure 8. Continued

(C_{ct}). The suggested simulated circuit for the non-corroded and corroded samples' corrosion mechanism is represented in Figure 9. Although non-corroded and corroded samples of the SS316L have a similar corrosion circuit, their parameter values of the resistance and capacitance tabulated in Table 7 are different.

The Bode and Nyquist diagrams of the S355 alloy revealed different corrosion mechanisms for the non-corroded and corroded samples. The Nyquist diagram of the non-corroded sample was characterised by a negative loop. As from the Bode diagram, negative phase angle and a decay of the impedance modulus were observed. For carbon steels, these behaviours were likely to associate with the adsorption of chloride and hydroxyl ions on surfaces (Gabrielli and Keddam 1992) (Yuan et al. 2010), (Hassen et al. 2013) (Price and Figueira 2017). Figure 10(a) presents the corrosion mechanism circuit of the non-corroded sample.

In the case of the corroded samples, the Bode and Nyquist diagrams showed diffusion process characteristics. Bode diagram of modulus impedance (*Zmod*) versus Frequency, exhibited a *Zmod* that increased with frequency reduction at 0.1–0.01 Hz. In the other Bode diagram, the phase angle (θ) versus Frequency, and the Nyquist diagram presented a positive tail at low frequencies that confirmed the diffusion process. Figure 10(b) shows the corrosion mechanism circuit of the corroded samples. Table 8 lists the electrochemical parameters and the S355 corrosion threshold values in artificial seawater.

Figures 7(d) and 8(d) illustrate the PPC's potential over time plots. These plots show the behaviour of cathodic and anodic branches of the SS316L and S355 when immersed in seawater.

The cathodic branch of the SS316L had an inclined behaviour with a low-slope because the cathodic reaction was controlled

Table 7. Corrosion Output Parameters and the threshold values of the SS316L in artificial seawater.

	Electrochemical Analysis Parameters						
	EN						
Sample	$I_{r.m.s}$ (A/cm^2)		R_n (Ω∗cm^2)			L.I.	
Non-Corroded	1.987E-8		1,645,815			0.026	
Corroded	3.570E-8		431,453			0.213	
	EIS						
	R_s (Ω∗cm^2)	R_{ct} (Ω∗cm^2)	C_{ct} (F/cm^2)	η_{ct}	R_{po} (Ω∗cm^2)	C_{po} (F/cm^2)	η_{po}
Non-Corroded	4.200	692,830	4.149E-5	0.90	62,452	1.739E-5	0.88
Corroded	4.000	290,600	3.477E-5	0.74	11,865	3.533E-5	0.90
	PPC						
	E_{corr} (V)	E_{bp}(V)	I_{corr} (A/cm^2)	I_{pass} (A/cm^2)	β_c (V/decade)	β_a (V/decade)	
	−0.152	0.380	6.785E-8	1.783E-7	−0.097	0.296	

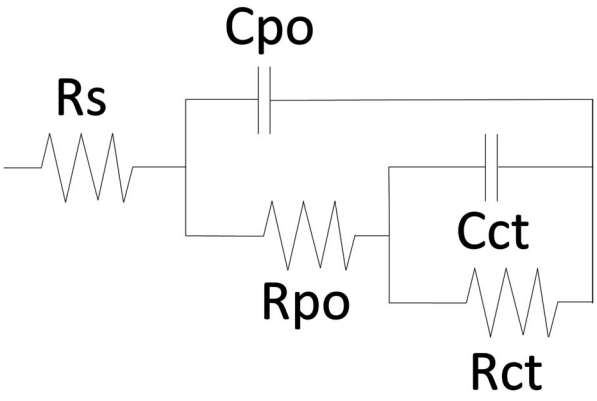

Figure 9. Corrosion mechanism circuit of the SS316L non-corroded and corroded samples from seawater immersion testing.

by the activation polarisation (Latha et al. 1998). Meanwhile, the anodic branch behaviour changed in according to the potential. A steep-slope was exhibited from −0.100 V to 0.380 V by the anodic branch. This was the potential range where the passive film was stable. Afterwards, the current density fluctuated with the potential until it reached 0.500 V, during which the cycle of corrosion pitting formation and re-passivation (metastable pitting) took place, similar to that observed by Yi et al. (2013). Re-passivation would not happen at ≥ 0.500 V causing a rapid rise of current density. The low current density in the passive region was associated with the low chemical activity of the passive film (Yi et al. 2013).

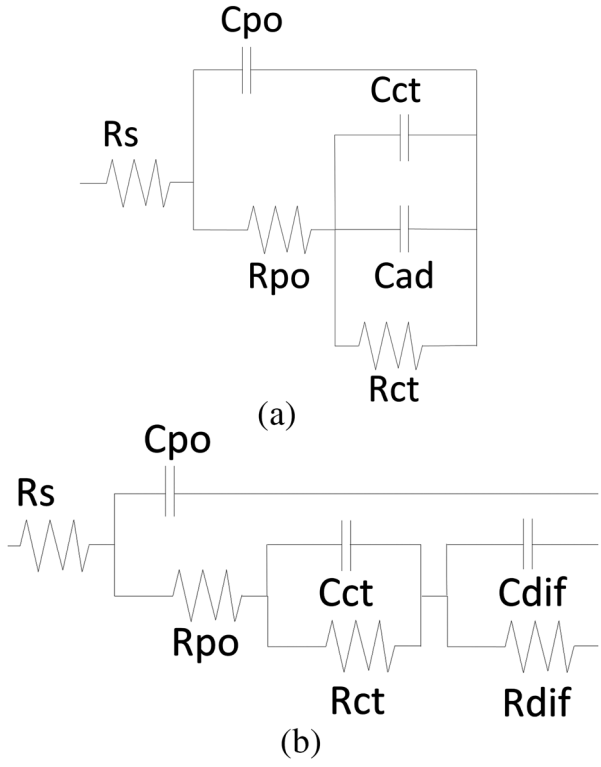

Figure 10. Corrosion mechanisms circuits of the S355 (a) non-corroded sample with a simulating adsorption–desorption process, and (b) corroded sample with a simulating diffusion processes from seawater immersion testing

Table 8. Corrosion output parameters and the threshold values of the S355 in artificial seawater.

	Electrochemical analysis parameters								
	EN								
Sample	$I_{r.m.s}$ (A/cm^2)			R_n (Ω∗cm^2)			L.I.		
Non-Corroded	7.258E−4			127			0.034		
Corroded	3.000E−3			63			0.100		
	EIS								
	R_s (Ω × cm^2)	R_{ct} (Ω × cm^2)	C_{ct} (F/cm^2)	η_{ct}	R_{po} (Ωcm^2)	C_{po} (F/cm^2)	η_{po}	C_{ad} (F/cm^2)	η_{ad}
Non-Corroded	3.900	266	3.597E−4	0.66	1412	7.906E−5	0.82	6.160E-3	0.16
Corroded	4.200	2737	2.611E−4	0.660	388	2.029E−4	0.800	R_{dif} (Ω × cm^2)	C_{dif} (F/cm^2)
								9475	3.722E−4
	PPC								
	E_{corr} (V)			I_{corr} (A/cm^2)		I_{diff} (A/cm^2)		β_c (V/decade)	β_a (V/decade)
	−0.643			1.456E-5		2.432E-5		−0.034	0.163

η_{dif} 0.720

The PPC analysis of the S355 from the artificial seawater immersion test indicated a vertical cathodic branch which suggested a cathodic reaction that was controlled by oxygen diffusion, similar to the work reported by Shi et al. (2017). On the anodic branch, the curve followed a horizontal path up to −0.550 V, before continuing with the inclined behaviour and raising to −0.380 V. This suggested that the anodic reaction was controlled by the activation polarisation (Gassama et al. 2015).

2. Conclusion

This paper discusses the industrial research demonstration stage of a proof-of-concept development of a low power wireless sensor network system for corrosion detection and monitoring offshore wind turbine parts/components, also known as *iWindCr*. The demonstration was in the format of a field trial where the *iWindCr* sensor system was installed to monitor and record changes of potential (voltage) and current density in real time of the M72 (10.9 galvanised steel) bolt, located at the MP-TP flanged connection of an offshore wind turbine in the UK south region. The system was installed just above the splash zone, meaning that the component/part monitored and the sensor system would never be fully immersed in seawater. This 30-day trial showed that the electrochemical analysis techniques (OCP and ZRA) adapted in the system were able to detect stable reading of the voltage and current density of the component in the moisture and salt spray condition. The sensor which has been designed to take reading at interval time in order to reduce power consumption was able to collect sufficient and meaningful data to allow for the determination of the corrosion state of the component/part. This was done by means of comparison with the corrosion threshold data that were generated from the exhaustive laboratory tests using mainly four different electrochemical analysis techniques (OCP, ZRA, EIS and PPC) as well as the verified/validated published data. The trial data can also be used to estimate the corrosion rate of the bolt, which is calculated currently at 4.1401E–15 cm/s.

The second part of the paper reported the generation of the *iWindCr* corrosion threshold data. The paper highlighted the electrochemical analysis process to determine the corrosion threshold parameters and values of SS316L and S235. It is necessary to utilise the four electrochemical analysis techniques to determine these materials' thresholds of different parameters. From the trial, it is learnt that corrosion threshold parameters and values will depend strongly on the environment where a component or material is exposed or subjected to. Referring to only one parameter such as a corrosion potential, could lead to the wrong interpretation or diagnostic of an outcome. The *iWindCr* system measures two parameters (voltage and current density), thus provides more confidence in the reliability of the method and system for detecting and monitoring corrosion.

Acknowledgement

The authors would also like to acknowledge the Faculty of Technology and the School of Mechanical and Design Engineering and School of Energy and Electronic Engineering, University of Portsmouth for their support in this work.

Disclosure statement

No potential conflict of interest was reported by the author(s).

Funding

This work was supported by the Innovate UK iWindCr Project (grant number 103504) and co-funded by our industrial partners Avonwood Development Ltd (Co. No. 02570711) and Avanti Communication Plc (Co. No. 03101607).

Notes on contributors

S. Simandjuntak is a senior lecturer at the School of Mechanical and Design Engineering (SMDE), UOP and the academic Principal Investigator (PI) in this project. Simandjuntak has interests and led research and innovation projects in relation to damage characterisation, structural integrity and life of engineering components.

N. Bausch is a senior lecturer at the School of Energy and Electronic Engineering (SENE) who has conducted research around sensor/multi-sensor integration.

A. Farrar is a technical staff at the SENE who has experience in sensor design and integration.

Juan Ahuir-Torres I was the appointed Research Associate in the iWindCr project and has research interest in tribology, surface and coating technology.

Bob Thomas is the director of Avonwood Developments. Avonwood delivers RFID solutions and technology.

Joseph Muna is a consultant at Avanti Communications Group Plc with the role to necessitate involvement in complete project lifespan - from user requirements, through system definition & design, development, testing and any post system delivery activities e.g. dissemination etc. Avanti is a satellite provider and operator.

ORCID

S. Simandjuntak http://orcid.org/0000-0003-3167-6882
N. Bausch http://orcid.org/0000-0001-9219-6052
Juan Ahuir-Torres I http://orcid.org/0000-0002-3160-0223

References

Ahuir-Torres JI, Bausch N, Farrar A, Webb S, Simandjuntak S, Nash A, Thomas B, Muna J, Jonsson C, Mathew D. 2019a. Benchmarking parameters for remote electrochemical corrosion detection and monitoring of offshore wind turbine structures. Wind Energy. 22:857–876.

Ahuir-Torres JI, Bausch N, Farrar AS, Webb S, Simandjuntak S, Nash A, Thomas B, Muna J, Jonsson C, Mathew D. 2019b. Corrosion threshold data of metallic materials in various operating environment of offshore wind turbine parts (tower, foundation, and nacelle/gearbox). Data in Brief, 25, pp 1–16, Elsevier.

Al-Fozan SA, Malik AU. 2008. Effect of seawater level on corrosion behavior of different alloys. Desalination. 228(1-3):61–67.

Arshad M, O'Kelly BC. 2013. Offshore wind-turbine structures: a review. Proceedings of the institution of civil engineers. Energy. *166*(EN4):139–152.

ASTM. 2013. Standard practice for the preparation of substitute ocean water. ASTM D1141-98. West Conshohocken, PA: ASTM International. www.astm.org.

Black AR, Mathiesen T, Hilbert LR. 2015. Corrosion protection of offshore wind foundations. Houston, TX: NACE International.

Burton T, Jenkins N, Sharpe D, Bossanyi E. 2011. Wind energy handbook. 2nd Edition. Chichester: John Wiley & Sons.

Choudhary S, Garg A, Mondal K. 2016. Relation between open circuit potential and polarization resistance with rust and corrosion monitoring of mild steel. J Mater Eng Perform. 25(7):2969–2976.

Compere C, Le Bozec N. 1997. *Behaviour of stainless steel in natural seawater. Paper presented at: The First Stainless Steel Congress in Thailand, Bangkok, Thailand, December 15-17, 1997.*

DNV. 2013. Design of offshore wind turbine structures. Standard DNV-OS-J101. Norway: Det Norske Veritas AS (DNV).

DNV. 2016. Corrosion protection for wind turbine. Standard DNVGL-RP-0416. Norway: Det Norske Veritas AS (DNV).

Estate C. 2010. A guide to an offshore wind farm. Power. 2010:1–70.

Estupiñán-López F, Almeraya-Calderón F, Margulis RB, Zamora MB, Martínez-Villafañe A, Gaona-Tiburcio C. 2011. Transient analysis of electrochemical noise for 316 and duplex 2205 stainless steels under pitting corrosion. Int J Electrochem Sci. 6:1785–1796.

Gabrielli C, Keddam M. 1992. Review of applications of impedance and noise analysis to uniform and localized corrosion. Corrosion. 48(10):794–811.

Gassama D, Diagne AA, Yade I, Fall M, Faty S. 2015. Investigations on the corrosion of constructional steels in different aqueous and simulated atmospheric environments. Bull Chem Soc Ethiop. 29(2):299–310.

Goyal N, Sandhu JK, Verma L. 2021. CDMA-based security against wormhole attack in underwater wireless sensor networks. In: Singh Hura G, Singh AK, Hoe LS, editors. Advances in communication and computational technology. Vol. 668. Singapore: Springer; p. 829–835.

Gupta O, Goyal N. 2021. The evolution of data gathering static and mobility models in underwater wireless sensor networks: a survey. J Ambient Intell Humaniz Comput. 1–17. https://doi.org/10.1007/s12652-020-02719-z.

GWEC. 2017. A Snapshot of top wind markets in 2017: Offshore Wind. Global Wind Energy Council 2017. Retrieved February 18, 2021. https://gwec.net/wp-content/uploads/2018/04/offshore.pdf.

Hassen SB, Bousselmi L, Rezrazi EM, Berçot P, Triki E. 2013. Corrosion behavior of carbon steel coated with magnesium electrodeposited from methyl magnesium chloride solution. J Coat Technol Res. 10(2):277–284.

Latha G, Rajendran N, Rajeswari S. 1998. Evaluation of superaustenitic stainless steels as construction materials in sea water service systems. J Mater Sci Lett. 17(6):519–522.

McCafferty E. 2010. Introduction to corrosion science. Alexandria: Springer.

Murata T. 2017. *Weathering steel*. In: Revie RW, editor. Uhlig's corrosion handbook. Third ed. Ottawa: Wiley, A Jonh Wiley & Sohns, Inc, Publications; p. 621–633.

Pawsey C. 2016. *Corrosion Protection for Offshore Wind, Prevention and Aftercare: Meet the Industry Players. 4th International Conference Corrosion Protection for Offshore Wind, Berlin, Germany*.

Perälä T. 2010. *Wind Power: the Material Requirements*. 2010.

Price SJ, Figueira RB. 2017. Corrosion protection systems and fatigue corrosion in offshore wind structures: current status and future perspectives. Coatings. 7(2):25.

RenewableUK. 2019. Retrieved February 18, 2021. https://www.renewableuk.com/page/WindEnergy.

Shi L, Qu SP, Chen HY, Yin YS, Yang LJ. 2017. *Tribocorrosion Behaviors of D40 Steel in Artificial Seawater. Paper presented at: Materials Science Forum* 2017.

Shreir LL. 1994. 1.6 – *localised corrosion*. In: Shreir LL, Jarman RA, Burstein GT, editors. Corrosion. Third ed. Oxford: Butterworth-Heinemann; p. 1:151–1:212.

Shreir LL, Jarman RA, Burstein GT. 2010. *3.2-Low-alloy steels*. In: Shreir LL, Jarman RA, Burstein GT, editor. Corrosion. Vol 1: metal/environment reaction. Third ed. Oxford: Butterworth-Heinemann; p. 23–33.

Sun Y. 2010. Corrosion behaviour of low temperature plasma carburised 316L stainless steel in chloride containing solutions. Corros Sci. 52(8):2661–2670.

UKWED. 2019. Retrieved February 18, 2021. https://www.renewableuk.com/page/UKWEDhome.

Umaya M, Noguchi T, Uchida M, Shibata M, Kawai Y, Notomi R. 2013. Wind power generation-development status of offshore wind turbines. Mitsubishi Heavy Ind Tech Rev. 50(3):29.

Weinell CE, Black AR, Mathiesen T, Nielsen PK. 2017. *New Developments in Coatings for Extended Lifetime for Offshore Wind Structures. Paper presented at: CORROSION* 2017.

Wharton J, Wood R. 2005. Flow corrosion behavior of austenitic stainless steels UNS S30403 and UNS S31603. Corrosion. 61(8):792–806.

Wind Europe. 2019. Offshore Wind in Europe: Key trends and statistic 2018. Windeurope.org. https://windeurope.org/wp-content/uploads/files/about-wind/statistics/WindEurope-Annual-Offshore-Statistics-2018.pdf (*retrieved on 18th February* 2021).

Xin S, Li M. 2014. Electrochemical corrosion characteristics of type 316L stainless steel in hot concentrated seawater. Corros Sci. 81:96–101.

Yi Y, Cho P, Al Zaabi A, Addad Y, Jang C. 2013. Potentiodynamic polarization behaviour of AISI type 316 stainless steel in NaCl solution. Corros Sci. 74:92–97.

Yuan XZ, Song C, Wang H, Zhang J. 2010. *EIS equivalent circuits*. In: Yuan XZ, Song C, Wang H, Zhang J, editor. Electrochemical Impedance Spectroscopy in PEM fuel cells: fundamentals and applications. Vol 1. Vancouver: Springer London Dordrecht Heidelberg New York; p. 139–191.